Article

# Nucleation and Growth of ZnO in Organic Solvents - an in Situ Study

C. Lizandara-Pueyo, M. W. E. van den Berg, A. De Toni, T. Goes, and S. Polarz

*J. Am. Chem. Soc.*, **2008**, 130 (49), 16601-16610 • DOI: 10.1021/ja804071h • Publication Date (Web): 14 November 2008



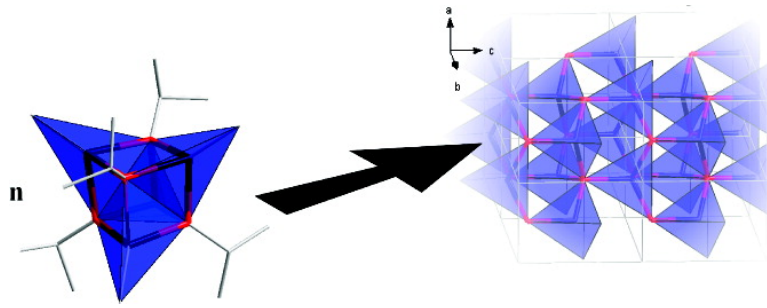

J|A|C|S
ARTICLES

Published on Web 11/14/2008

# Nucleation and Growth of ZnO in Organic Solvents - an in Situ Study

C. Lizandara-Pueyo,[†] M. W. E. van den Berg,[‡] A. De Toni,[‡] T. Goes,[†] and S. Polarz*,[†]

*Department of Chemistry, University of Konstanz, 78457 Konstanz, Germany, and Ruhr-University Bochum, Universitaestrausse 150, 44780 Bochum, Germany*

Received June 6, 2008; E-mail: sebastian.polarz@uni-konstanz.de

***Abstract:*** ZnO is a metal oxide material which possesses versatile properties and applications. Therefore, the target-oriented preparation of ZnO has become a major issue. Many preparation techniques involve bottom-up methods from precursor solutions. In the current contribution, a special precursor system is described that enables a fine-control of kinetic parameters for the nucleation and growth of ZnO in various organic solvents. A large variety of analytical techniques could be applied in an in situ fashion to probe for the ZnO formation at all times and all length scales. Among the analytical techniques are UV/vis, Raman, Fluorescence, X-ray absorption, $^1$H NMR-spectroscopy, dynamic light-scattering, and TEM. Three different regimes for nucleation and growth with different characteristics could be identified. Furthermore, the effect of different parameters on the resulting ZnO particle size was investigated.

## Introduction

Zinc oxide (ZnO) has become the most widely studied metal oxide material. The tremendous interest is provoked by the multifunctional character of ZnO, the option to vary its properties via the adjustment of morphology (size and shape), and the ease of synthesis of even very complex ZnO materials. It crystallizes in the Wurtzite structure. The $P_{63}mc$ crystal structure is unique due to its noncentrosymmetrical elemental cell possessing a hexad axis of symmetry. $P_{63}mc$ is a member of the polar crystal class. For such crystals particular surfaces exist corresponding to lattice planes containing only one type of atoms, either Zn or O. Thus, a ZnO crystal terminated by polar surfaces like the unreconstructed (0001)-surface ($Zn^{2+}$ terminated) and the (000$\bar{1}$)-surface ($O^{2-}$ terminated) exhibits a dipole moment along the crystallographic [0001] direction. As a consequence, ZnO is both pyroelectric and piezoelectric which represents the basis for applications as electromechanical or thermoelectrical coupling devices.[1] ZnO is a II−VI wide-gap semiconductor with a direct gap around 3.4 eV and an exciton binding energy of ∼60 meV. This makes ZnO a promising material for UV light-emitting-diodes (LEDs) and lasers.[2,3] In addition, ZnO is also used in solar cells,[4] field−emission displays, as a high-efficient green phosphor,[5] as an UV-photodetector material,[6] as a gas-sensor,[7,8] or varistor.[9] Apart from the mentioned, upcoming applications it is also important in large-scale products like in catalysis, respectively methanol synthesis over Cu/ZnO catalysts,[10−12] or in the rubber industry, or as an UV-blocker in sun-lotions.[13] A more comprehensive description of zinc oxide can be found in one of the recent, excellent review articles.[14]

Due to its importance and the potential of zinc oxide, it is obvious that enormous efforts have been made to explore expedient synthetic ways to ZnO with different particle size, various particle shapes and tailor-made hierarchical organization.

[†] Konstanz University.
[‡] Ruhr-University Bochum.

(1) (a) Look, D. C. *Mater. Sci. Eng., B* **2001**, *80*, 383. (b) Hickerne, *IEEE Trans. Microwave Theory Tech.* **1969**, *MT17*, 957.
(2) (a) Look, D. C.; Claftin, B. *Phys. Status Solidi B* **2004**, *241*, 624. (b) Look, D. C.; Reynolds, D. C.; Litton, C. W.; Jones, R. L.; Eason, D. B.; Cantwell, G. *Appl. Phys. Lett.* **2002**, *81*, 1830.
(3) Meyer, B. K.; Alves, H.; Hofmann, D. M.; Kriegseis, W.; Forster, D.; Bertram, F.; Christen, J.; Hoffmann, A.; Strassburg, M.; Dworzak, M.; Haboeck, U.; Rodina, A. V. *Phys. Status Solidi B* **2004**, *241*, 231.
(4) (a) Martinez, M. A.; Herrero, J.; Gutierrez, M. T. *Sol. Energy Mater. Sol. Cells* **1997**, *45*, 75. (b) Anderson, N. A.; Ai, X.; Lian, T. Q. *J. Phys. Chem. B* **2003**, *107*, 14414. (c) Keis, K.; Lindgren, J.; Lindquist, S. E.; Hagfeldt, A. *Langmuir* **2000**, *16*, 4688.
(5) Darici, Y.; Holloway, P. H.; Sebastian, J.; Trottier, T.; Jones, S.; Rodriquez, J. *J. Vac. Sci. Technol.* **1999**, *17*, 692.
(6) Monroy, E.; Omnes, F.; Calle, F. *Semicond. Sci. Technol.* **2003**, *18*, R33.
(7) Polarz, S.; Roy, A.; Lehmann, M.; Driess, M.; Kruis, F. E.; Hoffmann, A.; Zimmer, P. *Adv. Funct. Mater.* **2007**, *17*, 1385.
(8) Lin, H. M.; Tzeng, S. J.; Hsiau, P. J.; Tsai, W. L. *Nanostruc. Mater.* **1998**, *10*, 465.
(9) Clarke, D. R. *J. Am. Cer. Soc.* **1999**, *82*, 485.
(10) Peppley, B. A.; Amphlett, J. C.; Kearns, L. M.; Mann, R. F. *Appl. Catal., A* **1999**, *179*, 21.
(11) Polarz, S.; Strunk, J.; Ischenko, V.; Van den Berg, M.; Hinrichsen, O.; Muhler, M.; Driess, M. *Angew. Chem.* **2006**, *118*, 3031.
(12) Polarz, S.; Neues, F.; Van den Berg, M.; Grünert, W.; Khodeir, L. *J. Am. Chem. Soc.* **2005**, *127*, 12028.
(13) Fan, J.; Freer, R. *J. Appl. Phys.* **1995**, *77*, 4795.
(14) (a) Wang, Z. L. *J. Phys.: Condens. Matter* **2004**, *16*, R829. (b) Ozgur, U.; Alivov, Y. I.; Liu, C.; Teke, A.; Reshchikov, M. A.; Dogan, S.; Avrutin, V.; Cho, S. J.; Morkoc, H. *J. Appl. Phys.* **2005**, 98. (c) Klingshirn, C. *Phys. Status Solidi B* **2007**, *244*, 3027. (d) Klingshirn, C. *ChemPhysChem* **2007**, *8*, 782. (e) Woell, C. *Prog. Surf. Sci.* **2007**, *82*, 55.
(15) (a) Shiloh, M.; Gutman, J. *J. Cryst. Growth* **1971**, *11*, 105. (b) Hassani, S. S.; Lusson, A.; Tromson-Carli, A.; Ballutaud, D.; Didier, G.; Triboulet, R. *J. Cryst. Growth* **1999**, *207*, 30. (c) Sekiguchi, T.; Haga, K.; Inaba, K. *J. Cryst. Growth* **2000**, *214*, 68. (d) Ataev, B. M.; Bagamadova, A. M.; Djabrailov, A. M.; Mamedov, V. V.; Rabadanov, R. A. *Thin Solid Films* **1995**, *260*, 19. (e) Wu, J. J.; Liu, S. C. *Adv. Mater.* **2002**, *14*, 215.

  

ZnO can be prepared from the vapor phase using different methods including chemical vapor deposition,[15] or physical methods like RF magnetron sputtering, molecular-beam epitaxy or pulsed-laser deposition.[3,16] Despite that the mentioned methods furnish ZnO with very defined and interesting properties, their big disadvantage is regarding large-scale production. Larger amounts at significantly less technical effort can be provided using bottom-up techniques like precipitation/ crystallization from the liquid phase including melts.[17] The predominant precursor-type for zinc oxide are $Zn^{2+}$ salts combined with relatively primitive anions, mainly nitrate and acetate. The lowering of the pH value leads to the transient formation of zinc hydroxide which then transforms into ZnO by dehydration. As a consequence most studies about the formation of ZnO from solution have focused on water and other very polar solvents.[18,19] Good precursors for the generation of ZnO in organic solvents are organometallic zinc complexes. A nice study was published by Chaudret et al.[20] The authors were able to prepare monodisperse ZnO colloids from the controlled oxidation of diethylzinc ($ZnEt_2$) dissolved in tetrahydrofurane (THF). However, to the best of our knowledge there exists currently no mechanistic report about the nucleation and growth of ZnO in organic solvents. On the one hand, due to the excellent relevance of zinc oxide it is also very important to acquire a detailed knowledge about the formation of ZnO in nonaqueous systems. On the other hand, the free excess surface energy $\gamma_{L\leftrightarrow S}$ between the liquid and the forming solid plays a dominant role in all equations describing nucleation and growth. $\gamma_{L\leftrightarrow S}$ is directly influenced by the choice of the solvent. For instance, the free enthalpy for nucleation $\Delta G_N$ contains one surface and one volume term:

$$\Delta G_N = 4\pi r^2 \gamma_{L\leftrightarrow S} + \frac{4}{3}\pi r^3 \Delta G_{bulk} \quad (1)$$

with $\Delta G_{bulk}$ being the free enthalpy of the bulk:

$$\Delta G_{bulk} = \frac{-RT \ln S}{V_m} \quad (2)$$

with $V_m$ being the molar volume of the bulk crystal, and $S$ being the supersaturation.[21,22] The so-called supersaturation $S$ is the quotient of the actual concentration and the concentration of the respective species at equilibrium conditions. Therefore, $S$ indicates how far away from equilibrium the system is. The volume term in eq 1 is only important at small particle sizes due to its $r^2$ dependence in comparison to the $r^3$ dependence of the volume term. Therefore, $\gamma_{L\leftrightarrow S}$ is very important during nucleation and initial growth. $\gamma_{L\leftrightarrow S}$ can be varied if the nucleation experiments are accomplished in diverse solvents.

We present here a mechanistic study on the nucleation and growth of ZnO in organic, aprotic solvents. A special precursor system is employed which allows to perform a fine-tuning of nucleation and growth and, thus, permits to investigate the ongoing processes by in situ methods.

## Results and Discussion

**Setting up the System.** It was already mentioned that previous studies on ZnO formation from homogeneous solution have been performed on polar, protic solvents, most frequently on water.[18,19] $Zn^{2+}$-salts are of only limited use as far as apolar, aprotic solvents are concerned because their limited solubility in such media would not allow to reach a sufficiently high supersaturation level. The bis-alkylzinc compounds utilized by Chaudret et al. might be an alternative. However, the disadvantage of $ZnR_2$ is that they are difficult to handle due to the pronounced reactivity.[20] It would be very difficult to perform the nucleation and growth experiments under controlled conditions using bis-alkyzinc compounds as precursors for ZnO.

Our group introduced a different organometallic precursor system to ZnO materials chemistry recently: Alkylzincalkoxides with heterocubane architecture.[7,11,12,23−25] A large variety of the tetrameric compounds $[RZnOR']_4$ can be prepared from the reaction of $ZnR_2$ with the respective alcohol in high yield (see experimental part). The molecular zinc-oxo heterocubanes possess many advantages: They are highly soluble and stable in most aprotic and dry organic solvents. Due to their organometallic character they react to ZnO either by thermal reaction or the reaction with water.[12] It has to be stressed that in the latter case water does not the play the role of a solvent, it is a reactant. The reactivity of the $[RZnOR']_4$ compounds is much lower than the reactivity of the pure bis-alkylzinc compounds mentioned before, and it can be adjusted via the modification of the organic rests attached to the heterocubane core. Last but not least, the '$Zn_4O_4$' heterocubane core can be regarded as a preformed embryo for ZnO. The structure of $[MeZnO^{iso}Pr]_4$ for instance (determined from single-crystal analysis)[25] is plotted in Figure 1a in such a way that the central "$Zn_4O_4$" unit becomes visible. Furthermore, the tetrahedral coordination of the Zn-centers is highlighted which is also the coordination mode of zinc in ZnO. However, some differences between the precursor and ZnO-Wurtzite are also evident. The zinc-centered tetrahedra are linked to each other via edges for the molecular precursor and via angles in the Wurtzite crystal structure.

(16) (a) Sun, X. W.; Kwok, H. S. *J. Appl. Phys.* **1999**, *86*, 408. (b) Bagnall, D. M.; Chen, Y. F.; Shen, M. Y.; Zhu, Z.; Goto, T.; Yao, T. *J. Cryst. Growth* **1998**, *185*, 605. (c) Fujimura, N.; Nishihara, T.; Goto, S.; Xu, J. F.; Ito, T. *J. Cryst. Growth* **1993**, *130*, 269.

(17) (a) Sekiguchi, T.; Miyashita, S.; Obara, K.; Shishido, T.; Sakagami, N. *J. Cryst. Growth* **2000**, *214*, 72. (b) Reynolds, D. C.; Litton, C. W.; Look, D. C.; Hoelscher, J. E.; Claflin, B.; Collins, T. C.; Nause, J.; Nemeth, B. *J. Appl. Phys.* **2004**, *95*, 4802. (c) Ohyama, M.; Kozuka, H.; Yoko, T. *Thin Solid Films* **1997**, *306*, 78. (d) Meulenkamp, E. A. *J. Phys. Chem. B* **1998**, *102*, 5566.

(18) (a) Wong, E. M.; Bonevich, J. E.; Searson, P. C. *J. Phys. Chem. B* **1998**, *102*, 7770. (b) Viswanatha, R.; Sapra, S.; Satpati, B.; Satyam, P. V.; Dev, B. N.; Sarma, D. D. *J. Mater. Chem.* **2004**, *14*, 661.

(19) (a) Turgeman, R.; Tirosh, S.; Gedanken, A. *Chem.−Eur. J.* **2004**, *10*, 1845. (b) Uthirakumar, P.; Lee, Y. S.; Suh, E. K.; Hong, C. H. *Phys. Lett. A* **2006**, *359*, 223. (c) Viswanatha, R.; Amenitsch, H.; Sarma, D. D. *J. Am. Chem. Soc.* **2007**, *129*, 4470. (d) Viswanatha, R.; Santra, P. K.; Dasgupta, C.; Sarma, D. D. *Phys. Rev. Lett.* **2007**, 98.

(20) (a) Monge, M.; Kahn, M. L.; Maisonnat, A.; Chaudret, B. *Angew. Chem., Int. Ed.* **2003**, *42*, 5321. (b) Kahn, M. L.; Monge, M.; Colliere, V.; Senocq, F.; Maisonnat, A.; Chaudret, B. *Adv. Funct. Mater* **2005**, *15*, 458. (c) Kahn, M. L.; Monge, M.; Snoeck, E.; Maisonnat, A.; Chaudret, B. *Small* **2005**, *1*, 221. (d) Kahn, M. L.; Cardinal, T.; Bousquet, B.; Monge, M.; Jubera, V.; Chaudret, B. *ChemPhysChem* **2006**, *7*, 2392.

(21) Mullin, J. W. *Crystallization*, 3rd ed.; Oxford University Press: Oxford, 1997.

(22) Park, J.; Soon, J. J.; Kwon, S. G.; Jang, Y.; Hyeon, T. *Angew. Chem., Int. Ed.* **2007**, *46*, 4630.

(23) (a) Polarz, S.; Orlov, A.; Schüth, F.; Lu, A. H. *Chem.−Eur. J.* **2007**, *13*, 592. (b) Orlov, A.; Roy, A.; Lehmann, M.; Driess, M.; Polarz, S. *J. Am. Chem. Soc.* **2007**, *129*, 371. (c) Polarz, S.; Roy, A.; Merz, M.; Halm, S.; Schröder, D.; Scheider, L.; Bacher, G.; Kruis, F. E.; Driess, M. *Small* **2005**, *1*, 540. (d) Polarz, S.; Orlov, A.; Van den Berg, M.; Driess, M. *Angew. Chem., Int. Ed.* **2005**, *44*, 7892. (e) Roy, A.; Polarz, S.; Rabe, S.; Rellinghaus, B.; Zahres, H.; Kruis, F. E.; Driess, M. *Chem.−Eur. J.* **2004**, *10*, 1565.

(24) Van den Berg, M.; Polarz, S.; Tkachenko, O. P.; Klementiev, K. V.; Bandyopadhyay, M.; Khodeir, L.; Gies, H.; Muhler, M.; Grünert, W. *J. Catal.* **2006**, *241*, 446.

(25) Ischenko, V.; Polarz, S.; Grote, D.; Stavarache, V.; Fink, K.; Driess, M. *Adv. Funct. Mater.* **2005**, *15*, 1945.

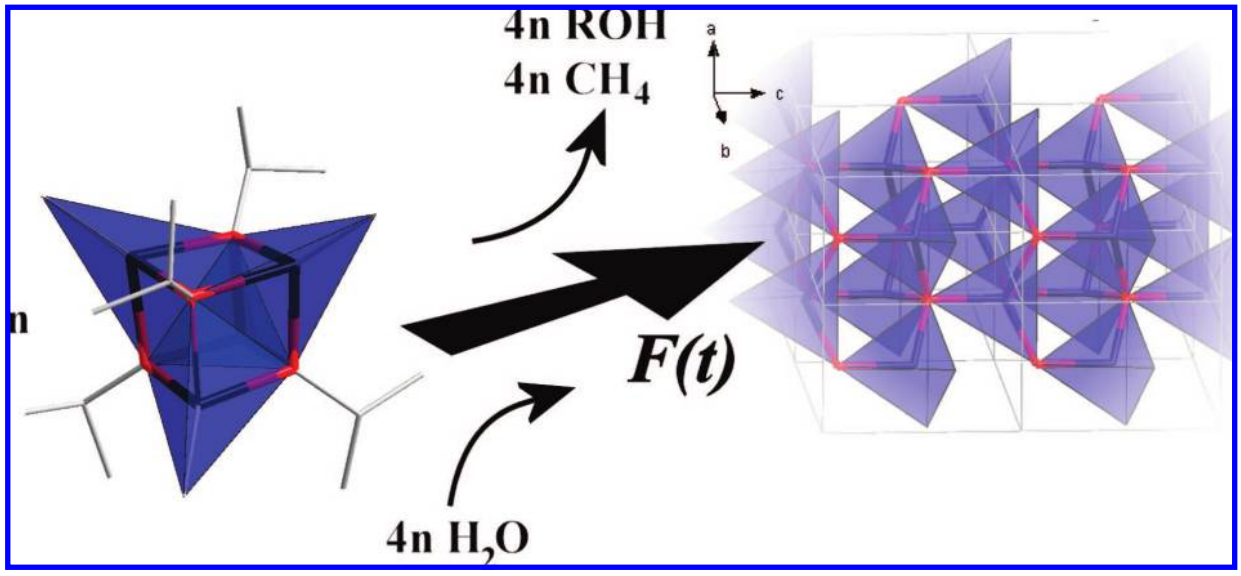


***Figure 1.*** Generation of ZnO with Wurtzite crystal structure from the reaction of the organometallic zinc-oxo heterocubanes precursors with water is imaged. The molecular structure of the heterocubane $[MeZnO^{iso}Pr]_4$ (H-atoms omitted) is shown exemplarily for the precursor class. Zinc atoms, black; oxygen atoms, red; carbon atoms, gray. The "$Zn_4O_4$" core is highlighted by the thick bonds. Furthermore, the tetrahedral coordination of zinc is indicated by the blue, translucent coordination polyeders. The vertices of each tetrahedron are given by three oxygen atom and one $^{-}CH_3$-group.

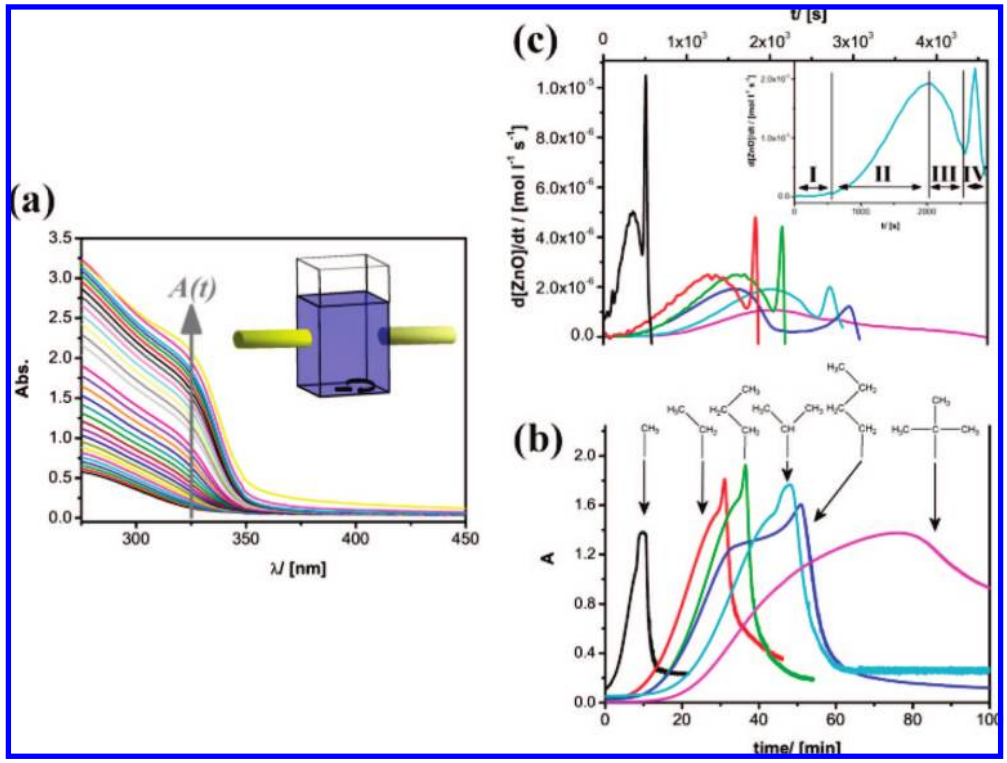


***Figure 2.*** (a) UV−vis absorption spectra measured in transmission modus for the reaction of $[MeZnO^{iso}Pr]_4$ with water in THF as a solvent ($c = 8 \cdot 10^{-4}$ mol/L; $T$ = rt). (b) Absorption values as a function of time measured at a fixed wavelength of $\lambda = 350$ nm for different heterocubanes $[MeZnOR]_4$. (c) Reaction rate as a function of time.

The formation of ZnO can be followed by optical spectroscopy in the UV/vis region, absorption and fluorescence measurements, by dynamic light scattering (DLS), and powder X-ray diffraction (PXRD). Different heterocubanes $[MeZnOR']_4$ with $R' = CH_3 \approx$ Me, $CH_2CH_3 \approx$ Et, $CH_2CH_2CH_3 \approx$ Pr, $CH(CH_3)_2 \approx {}^{iso}$Pr, $CH_2CH_2CH_2CH_3 \approx$ Bu, $C(CH_3)_3 \approx {}^{tert}$Bu have been synthesized (see Experimental Section and Supporting Information S-1). Solutions in tetrahydrofurane (THF) were prepared and an equimolar amount of water with respect to ZnMe-groups was added using a cuvette as a reaction vessel (see Figure 2a). UV/vis spectra were recorded under constant stirring. With time the evolution of an absorption edge can be seen. Because all other products of the reaction between the heterocubanes and water do not possess an absorption band above $\lambda = 250$ nm, the absorption band can be correlated to the appearance of zinc oxide. A significant blue-shift of the adsorption edge to $\lambda \approx 325-360$ nm in comparison to bulk-ZnO ($\lambda_{gap} \approx 380$ nm) is found which can be explained by a quantum-size effect caused

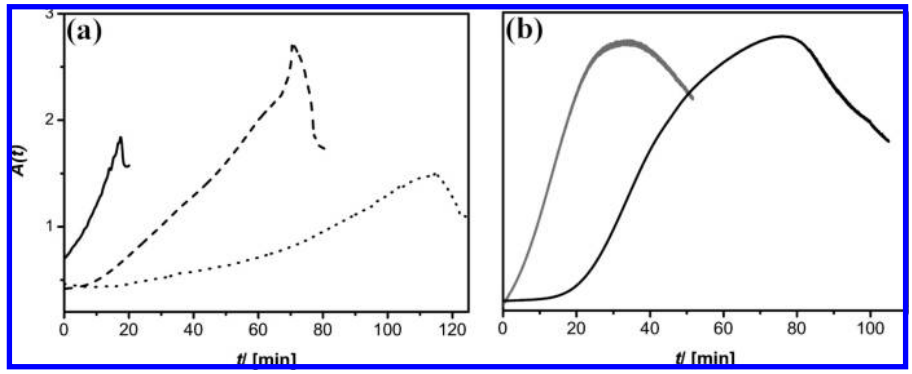


***Figure 3.*** Temperature dependency (a; $T = 10$ °C → dotted line; $T = 25$ °C → dashed line; $T = 33$ °C → solid line; $c = 8 \cdot 10^{-4}$ mol/L) and concentration dependency (b; $c = 8 \cdot 10^{-4}$ mol/L → black line; $c = 1.2 \cdot 10^{-3}$ mol/L → gray line) of the reaction of $[MeZnO^{tert}Bu]_4$ with water.

by very small ZnO particles[18,26] The UV−vis data, respectively the absorption as a function of time $A(t)$ should give valuable information about the formation of ZnO (eq 3).

$$A(t) \rightarrow v = \frac{dc_{ZnO}(t)}{dt} = k_{ges} \cdot C_{[MeZnOR]_4}(t)^{n1} \cdot C_{H_2O}(t)^{n2} \quad (3)$$

with $k_{ges}$ being the reaction rate constant and $n_{1/2}$ being the reaction orders. Therefore, kinetic data were recorded at a fixed wavelength $\lambda = 325$nm for all the heterocubanes mentioned (Figure 2a). The result is shown in Figure 2b. The organic group shielding the "$Zn_4O_4$" core has a significant impact on the rate of ZnO formation. The $[MeZnOMe]_4$ heterocubane reacts very rapidly. The reaction is finished after 15min. The more shielded the inorganic core of the precursor is the slower becomes the process. The reaction of $[MeZnO^{tert}Bu]_4$ is not completely finished even after 100 min. According to eq 3 two further possibilities exist to alter the rate of the reaction. These are to change the reaction rate constant or the concentration of at least one precursor (Figure 3b). A change in temperature (Figure 3a) alters the reaction rate constant according to Arrhenius law (eq 4).

$$k_{ges} = k^0_{ges} \exp\left(-\frac{E_{A,ges}}{RT}\right) \quad (4)$$

with $E_{A,ges}$ being the activation barrier. The presented data indicate that the chosen system allows for the fine-tuning of kinetic factors in such a way that a large variety of analytical techniques can be applied for a detailed in situ investigation of homogeneous nucleation and growth of ZnO from the mentioned molecular precursors. A particularly slow reaction can be realized for $[MeZnO^{tert}Bu]_4$ as a precursors at low temperature and at low concentration.

**In situ Investigation of Homogeneous ZnO Nucleation and Growth.** It is necessary for the nucleation of ZnO that a sufficiently high supersaturation builds up,[22] originating from the reaction of the molecular precursor with water during the initiation period of the entire process. At this point it is valuable to see the experiments discussed in the current paper also in the context of knowledge reported in sol−gel process science.[27] Unlike to silica and organosilica materials, there are only limited mechanistic studies on the formation of transition metal oxides via the sol−gel process.[28] Much of the attention has focused on pure metal alkoxide systems as sol−gel precursors, eventually stabilized by nucleophilic, oxygen donor ligands.[29] Organometallic precursors have been used for sol−gel processes very rarely which makes it very difficult to relate previous findings to the study presented here. However, it is well established for the hydrolysis of transition metal alkoxides containing additional, stabilizing ligands that the less electronegative ligands are cleaved first and then the more electronegative ligands. Regarding our system, the alkyl zinc alkoxides, it can be expected that the $CH_3$ ligand is less electronegative than the OR ligand. Therefore, a chemically reasonable suggestion is that water will react rapidly with the $Zn^+-CH_3^-$ group leaving Zn−OH behind. Zn−OH groups will polycondensate to Zn−O−Zn entities accompanied by water elimination (for better illustration, the discussed mechanism is shown in the Supporting Information S-2). $^1$H NMR spectroscopy is a suitable technique to check the latter hypothesis because the current process is accomplished in the homogeneous phase. In-situ $^1$H NMR measurements recorded in deuterated THF are shown in Figure 4a. Signals for residual, nondeuterated THF ($\delta = 3.58$, 1.72 ppm), for the heterocubane precursor ($\delta = -0.47$, 1.35 ppm), for the products of the reaction methane and tert-butanol ($\delta =$ 0.14, 1.13, 3.66 ppm) and for an intermediate species ($\delta =$ −0.91 ppm) can be observed. Additional information was acquired in the following way: First, each of the above-mentioned signals was integrated as a function of time. Then, a normalization procedure was performed. The signals corresponding to the precursors were set to $I_{norm} = 100\%$ at $t = 0$ min and the signals corresponding to products were set to $I_{norm} = 100\%$ at $t = 60$ min. This procedure allows a comparison of consumption and emergence of different species to each other (see Figure 4b).

The findings from $^1$H NMR are supported by FT-Raman spectra recorded for the reaction of $[MeZnO^{tert}Bu]_4$ with water under similar conditions (see Supporting Information S-3). Raman spectroscopy can also be applied as an in situ technique in the current case because all heterocubanes precursors possess well defined Raman spectra (see Supporting Information S-4). Furthermore, FT-Raman is also fast enough in comparison to the relevant time scale (a spectrum of sufficient quality can be recorded within 15 s), and water and hydroxo-groups are not visible in Raman. The FT-Raman spectrum of $[MeZnO^{tert}Bu]_4$ is shown in Supporting Information S-4. In the accessible spectral window in THF (800−200 cm$^{-1}$) which was used as a

(26) Steigerwald, M. L.; Brus, L. E. *Acc. Chem. Res.* **1990**, *23*, 183.
(27) Brinker, C. J.; Scherer, G. W. *Sol-Gel Science: The Physics and Chemistry of Sol-Gel Processing*, 1st ed.; Academic Press Inc: London, 1990.
(28) (a) Livage, J.; Sanchez, C.; Henry, M.; Doeuff, S. *Solid State Ionics* **1989**, *32−33*, 633. (b) Livage, J.; Henry, M.; Sanchez, C. *Prog. Solid State Chem.* **1988**, *18*, 259.
(29) (a) Mehrotra, R. C.; Singh, A. *Prog. Inorg. Chem.* **1997**, *46*, 239. (b) Hubert-Pfalzgraf, L. G. *J. Mater. Chem.* **2004**, *14*, 3113.

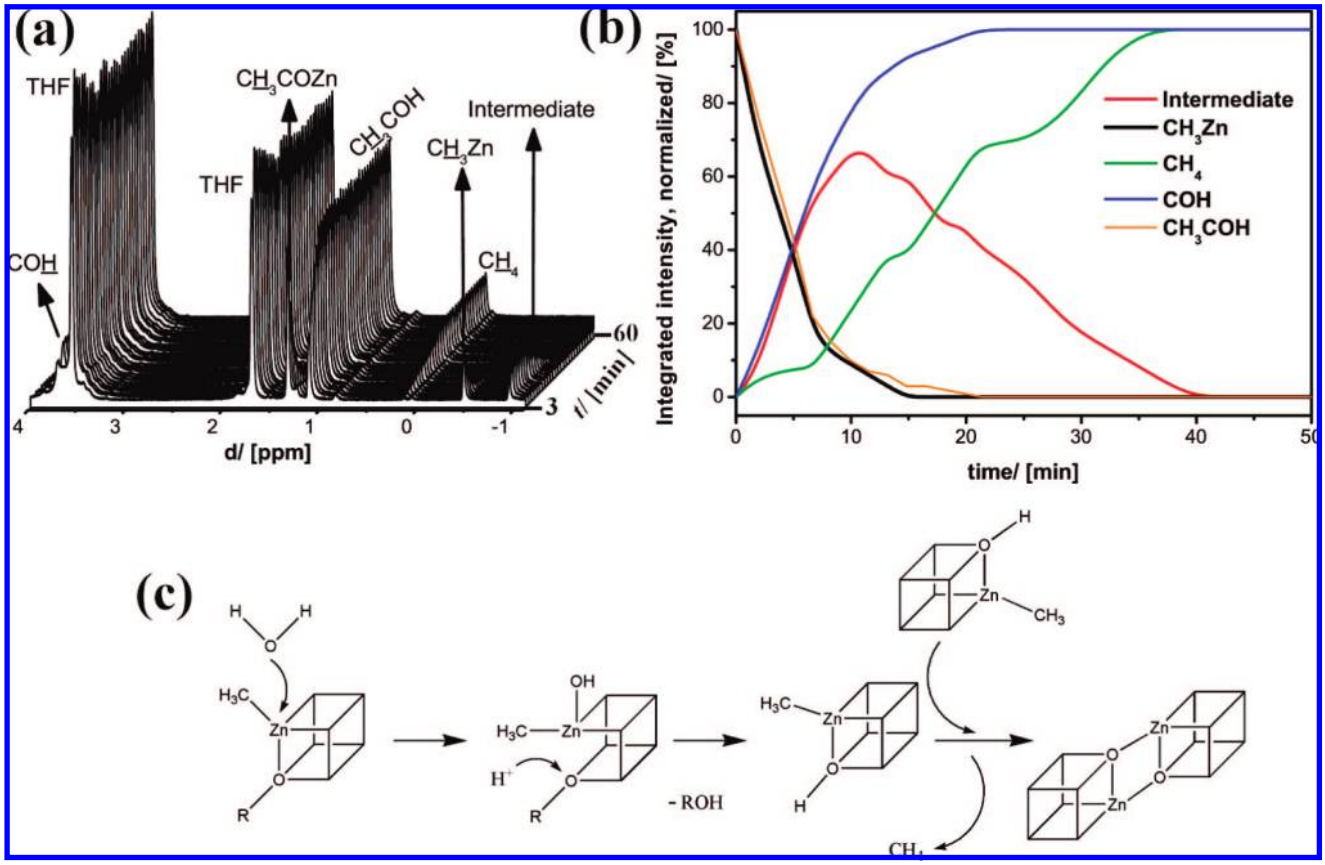


***Figure 4.*** (a) In situ $^1$H NMR spectra of the reaction of $[MeZnO^{tert}Bu]_4$ with water in deuterated THF as as a solvent. (b) Integrated, normalized intensity of the signals corresponding to important species in the reaction plotted as a function time. (c) Proposed mechanism. For better visibility all groups except the ones directly reacting are shown as edges in the heterocubane structure.

solvent, this particular precursor exhibits five characteristic bands. Comparison to the Raman spectra of the alternative $[MeZnOR]_4$ compounds reveals that the bands at $\bar{\nu}_1 = 220$ cm$^{-1}$, and $\bar{\nu}_2 = 547$ cm$^{-1}$ correlate to the "$Zn_4O_4$" core because they are present in all precursors. The bands at $\bar{\nu}_3 = 480$ cm$^{-1}$ and $\bar{\nu}_4 = 771$ cm$^{-1}$ are specific for the O$^{tert}$Bu-group, and the band at $\bar{\nu}_5 = 383$ cm$^{-1}$ correlates to a "ZnO−C−C" entity. Expectedly, the bands $\bar{\nu}_1$ vanish with time and a new band at $\bar{\nu}_6 = 750$ cm$^{-1}$ appears right at the beginning of the reaction. This new bands originates from the free alcohol tert-butanol. Interestingly, the band at $\bar{\nu}_5 = 383$ cm$^{-1}$ does not vanish completely. This might indicate that some O$^{tert}$Bu groups remain bound on the surface of the ZnO-particles.

Summarizing the results from both analytical methods, one can say: Unlike to the expectations from the literature on sol−gel processes, the Zn−$CH_3$ function is not consumed prior to the alkoxide group (Figure 4b). The free alcohol is formed already at the beginning of the reaction, although it is known for various alkoxide sol−gel precursors that the steric demand of the tert-butyl group stabilizes the metal−oxygen bond. The emergence of methane occurs later than expected and is coupled to the degradation of the intermediate species (Figure 4b). The mechanism that was proposed before (see also Supporting Information S-2) seems to be incorrect because it requires the immediate consumption of ROZn−$CH_3$ accompanied by the immediate formation of $CH_4$. The occurrence of the $^1$H NMR signal at low field for the intermediate species indicates that still some sort of $[XOZn-CH_3]_x$ entity is present. Furthermore, the intermediate species is formed simultaneously to the release of the free alcohol. Although we can not rule out for sure that the cleavage of the Zn−OR bond might be the first step of the reaction, our data appear to be most consistent with a nucleophilic attack of water at the Lewis-acidic $Zn^{2+}$ center (Figure 4c) forming a penta-coordinated species. The released proton attacks the alkoxide group and induces the formation of the alcohol. Further, it is reasonable to assume that the "$Zn_4O_4$" oxocluster now possesses one OH corner instead of O$^{tert}$Bu. The latter intermediate is unstable against the reaction with a second intermediate. Two Zn−O−Zn bonds are formed in the next step and methane is released. The discussed mechanism shown in Figure 4c is also consistent with the observation that the alkoxide group has a profound impact on the kinetic of ZnO formation shown in Figure 2b. To derive the dependence of the reaction rate with time it is necessary to extract quantitative information from the UV−vis data. Using Lambert−Beers law (eq 5) it should be possible to transform the measured adsorption values $A(t)$ into the corresponding concentration values for ZnO in solution ($c_{ZnO}(t)$).

$$A(t)_{\lambda=325nm} = \varepsilon_{\lambda=325nm} \cdot c_{ZnO}(t) \cdot d \qquad (5)$$

with $\varepsilon_{\lambda=325nm}$ being the extinction coefficient at $\lambda = 325$nm and $d$ being the inner extension of the cuvette = 10.000 mm. Obviously $\varepsilon_{\lambda=325nm}$ is required first. Therefore, $\varepsilon_{\lambda=325nm}$ was determined from an independent experiment. A reference system containing ZnO colloids in a similar size range was prepared and used to acquire a calibration curve for the extinction coefficient of ZnO in homogeneous solution (see Supporting Information S-5). The preparation of the colloidal ZnO solutions is behind the scope of the current manuscript and will be presented elsewhere. The extinction coefficient was determined

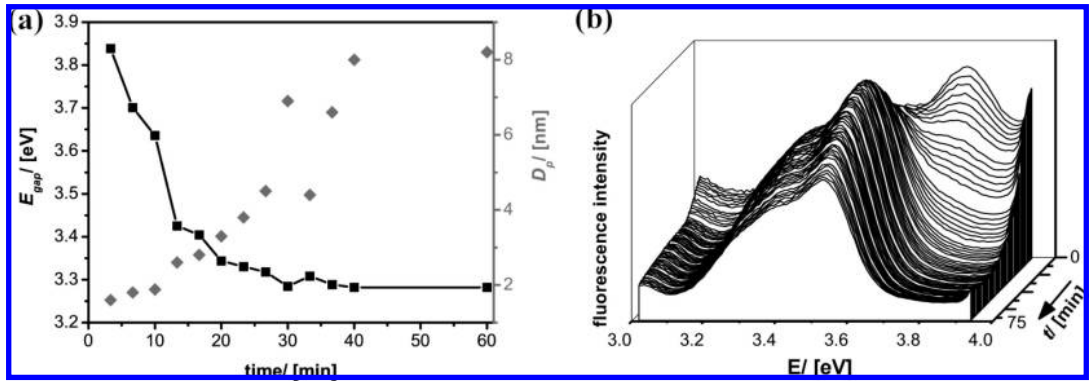


***Figure 5.*** (a) Time-dependent development of the band gap energy of ZnO formed from the reaction of $[MeZnO^{tert}Bu]_4$ with water ($c = 8 \cdot 10^{-4}$ mol/L, $T = 25$ °C), and the ZnO particle size (gray points) determined from $E_{gap}$. Fluorescence spectra monitoring the same process are shown in (b).

to $\varepsilon_{\lambda=325nm} = 6.6859 \cdot 10^4$ L·mol$^{-1}$·m$^{-1}$. The first derivative of $A(t)$ is the reaction rate $v$ (eq 3). The plot of $v$ against time reveals similarities in the kinetic behavior independent from the type of heterocubane used. Four phases can be identified. In the first phase, the initiation period, very limited ZnO is formed. During this phase the molecular reactions discussed in the previous chapter are progressing until a sufficiently high supersaturation is reached. Then, the ZnO formation rate speeds up until a maximum is reached (phase II). At the short wavelength ($\lambda = 325$ nm) used, the formation of even very small ZnO particles can be observed. Therefore, phase II can be attributed to the nucleation process. The remaining ZnO-embryos ($\approx$ molecular precursors) are consumed during phase III. Surprisingly, for a short moment the ZnO formation rate appears to increase again in phase IV. However, this is a virtual increase because a visual inspection of the cuvette indicates that the solution becomes first turbid and then flocculates in phase IV. The second maximum in Figure 2c can be explained by the enhanced scattering of the solution containing dispersed, reflecting particles. Because the experiments were performed in transmission modus, less light reaches the detector. When flocculation occurs and particles begin to sediment, more light is transmitted and the absorption decreases again. The flocculation is reasonable because we have not used any stabilization agent during the experiments.

The absorption spectra shown in Figure 2a contain further information. According to the effective mass (EM) model introduced by Brus the band gap of semiconductor nanoparticles depends on crystal size $D_p$ like described in eq 6:[26,30]

$$E_{gap}(D_p) = E^0_{gap} + k\frac{\hbar^2\pi^2}{2D_p^2} - \frac{1.8e^2}{4\pi \in \in_{0D_p}} - k' \qquad (6)$$

with $E^0_{gap}$ being the band gap of bulk ZnO $= 5.39 \cdot 10^{-19}$ J (3.37 eV), $\varepsilon_0$ being permittivity of free space, $\varepsilon$ being the relative permittivity $= 3.7$, e being the electric charge, $k = 7.01 \cdot 10^{30}$ ms$^{-1}$, and $k' = 6.81 \cdot 10^{21}$ J.[31] To verify that the effective mass model is applicable to the samples described in the current study, different ZnO materials were prepared as reference samples, the band gap was determined by UV/vis measurements and the crystal size was determined from PXRD data. Then, the results were compared to the EM-model, revealing a good agreement (see Supporting Information S-6). It is seen that the derivation from the band gap of bulk ZnO represents a very sensitive measure for particle sizes below $D_p \approx 4$ nm due to the significant blue-shift in this region. Therefore, UV/vis spectroscopy is a suitable technique to investigate the nucleation process in the early stages of the process. The values for $E_{gap}$ and $D_p$ calculated from the EM model are shown in Figure 5a for different times during the formation of ZnO. During the first 20 min of the reaction ZnO particles with $D_p = 1.5-2$ nm are found, which we attribute to the critical nuclei. Then, the particle size rises constantly up to $D_p \approx 8$ nm. The conclusions made from UV/vis spectroscopy are furthermore supported by in situ fluorescence spectroscopy shown in Figure 5b. The fluorescence signal at $\lambda = 350$ nm vanishes in the beginning of the reaction and can therefore be associated to the heterocubane $[MeZnO^{tert}Bu]_4$. A new signal forms at $\lambda = 367$ nm and then decays again (see Supporting Information S-7). Therefore, the fluorescence signal at $\lambda = 367$ nm should be connected to the formation of the critical nuclei. Finally, a third fluorescence signal with steadily increasing intensity forms at $\lambda \approx 377$ nm which can be attributed to larger ZnO particles. It should also be noted that a fourth fluorescence signal, the so-called defect-luminescence was detected at $\lambda = 550$ nm.[25]

So far no information about the internal structure of the critical nuclei (CN) was accessible. Because their size is below 2 nm the application of PXRD is not an option for further investigation of the CN. On the other hand, X-ray absorption spectroscopy (XAS) enables to probe very small particles. The X-ray Absorption Near Edge Structure (XANES) of the Zn K-edge probe unoccupied p-like states of the first nearest neighbors and are thus highly sensitive to both the ligand type, the symmetry surrounding the central atom, and the observed changes in the first-shell environment of the central zinc atom. Based on the knowledge about our system and the kinetic factors the experimental parameters were adjusted in such a way that XAS data could be acquired (see Experimental Section) during the period when nucleation takes place ($t_1$), when growth takes place ($t_2$) and when the process is nearly finished ($t_3$). The XANES of the progressing reaction, compared to bulk ZnO as a reference is shown in Figure 6a and the EXAFS in Figure 6b. The XANES of bulk ZnO is characterized by five features $E_{1;shoulder} = 9663$ eV, $E_2 = 9668$ eV, $E_3 = 9679$ eV, $E_4 = 9714$ eV and $E_5 = 9738$ eV. The unsplit peak $E_2$ is the main and most intense shape resonance and constitutes the typical whiteline feature.[32] Peak $E_3$ is typical of $Zn^{2+}$ in a tetrahedral

(30) (a) Brus, L. E. *J. Chem. Phys.* **1983**, *79*, 5566. (b) Brus, L. E. *J. Chem. Phys.* **1984**, *80*, 4403. (c) Rosetti, R.; Ellison, J. L.; Gibson, J. M.; Brus, L. E. *J. Chem. Phys.* **1984**, *80*, 4464.
(31) Brus, L. E. *J. Nanostruct. Mater.* **1992**, *1*, 71.
(32) Larcheri, S.; Armellini, C.; Rocca, F.; Kuzmin, A.; Kalendarev, A.; Dalba, G.; Graziola, R.; Purans, J.; Pailharey, D.; Jandard, F. *Superlattices Microstruct.* **2006**, *39*, 267.

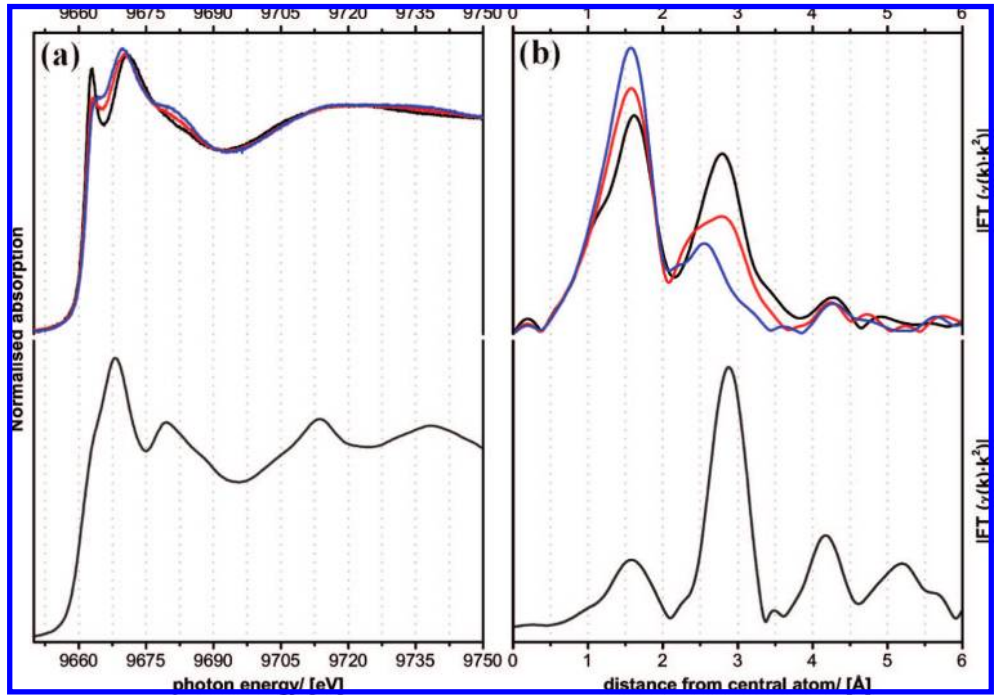


***Figure 6.*** (a) Zn−K XANES and (b) EXAFS for the reaction of $[MeZnO^{tert}Bu]_4$ with water. The nucleation period (black), the growth period (red) and at the end of the reaction (blue). Bulk ZnO as a reference is shown in dark gray (bottom graph).

environment, as studies on solvated zinc clusters have shown.[33] The two distinct features $E_4$ and $E_5$ are EXAFS-like in nature, but are highly dependent on the first coordination shell. The distance between features $E_4$ and $E_5$ is indicative (in an empirical sense) for the metal−ligand distance.[34] The XANES recorded during the nucleation period ($t_1$) is markedly different to the reference sample ($E_1(t_1) = 9663$ eV; $E_2(t_1) = 9671$ eV; $E_3(t_1) = 9685$ eV; $E_4(t_1) = 9722$ eV; $E_5(t_1) =$ missing). The signal at $E_1$ which is indicative for an anisotropic coordination shell around $Zn^{2+}$ centers possesses pronounced intensity.[33] The assumption of an asymmetric, tetrahedral coordination is reasonable because due to the restricted size of the critical nuclei a significant amount of atoms are automatically located at the surface. Then, these zinc atoms are centers which are bound to OH or alkoxide groups (which have been found be FT-Raman spectroscopy; see above) at the surface and Zn−O(Zn) in direction of the volume of the nucleus. The presence of surface groups is supported by EXAFS (Figure 6b). An additional shoulder appears in the first coordination shell around the zinc atoms at a distance of 1.1 Å. It is known for semiconductor not that localized variations in electronic properties are induced by the presence of an interface, and that one has to expect significant surface reconstructions. Such surface reconstructions result frequently in the shortening of bonding distances between the atoms in the first and second surface layers. Furthermore, it is seen that the distances for shells around the central Zn center is comparable to the pattern found for bulk ZnO. As a consequence, it seems that the critical nuclei already have Wurtzite structure. With time the intensity of the peak $E_1$ decreases until at $t_3$ the entire XANES (Figure 6a) is very close to bulk ZnO. The EXAFS (Figure 6b) for $t_2$ is a superposition of the features of $t_1$ and $t_3$ indicating that grown nanoparticles and still some critical nuclei are present. Close to the end of the reaction the Zn−O shell consists of merely "framework" zinc-to-oxygen contributions, and as a result the Zn−O peak becomes narrower and increases in amplitude. The final stage is characterized by an even stronger increase of the Zn−O amplitude, whereas the Zn−Zn shell has shifted to 2.55 Å. In comparison, the bulk zinc oxide sample has Zn−Zn shell at 2.87 Å. The difference can be explained by the nanoparticulate character of the zinc oxide phase which is in good agreement to the literature.[24]

The formation of particles can also be followed by dynamic light scattering (DLS) measurements. The results are shown in Figure 7a. Until $t \approx 20$ min there is no formation of particles which is in good agreement with the length of the initiation period deduced from UV−vis measurements. It should be noted that it is not possible to detect the critical nuclei ($D_p > 2$nm) with our DLS equipment. Then, the formation of ZnO particles $\approx 4$ nm in size occurs which further grow to $\approx 8.4$ nm which is also in good agreement with the particle sizes deduced from in situ UV−vis measurements (Figure 5a). The 8.4 nm large particles are present almost until the end of the reaction ($t =$ 85 min), however, they vanish finally. Simultaneously to the primary growth process there is secondary growth as soon as the primary particles are formed. Larger aggregates are found, and the size of these aggregates increases steadily until 190 nm at $t = 105$ min. The solution has become turbid at this point and precipitation of ZnO occurs at $t > 110$ min. Simultaneous to the DLS measurement samples were taken from the solution, one drop was placed on a carbon coated copper carbon grid and the grid was immediately dried in a desiccators by applying oil-pump vacuum. Then, the samples were analyzed with transmission electron microscopy (TEM) shown in Figure 7 and Supporting Information S-6. After $t = 30$ min some ZnO particles have formed. The aggregation state is rather low and

(33) Takahashi, M.; Tanida, H.; Kawauchi, S.; Harada, M.; Watanabe, I. *J. Synchroton Rad.* **1999**, *6*, 278.
(34) Zhao, W.; Chu, W. S.; Yang, F. F.; Yu, M. J.; Chen, D. L.; Guo, X. Y.; Zhou, D. W.; Shi, N.; Marcelii, A.; Niu, L. W.; Teng, M. K.; Gong, W. M.; Benfatto, M.; Wu, Z. Y. *Nucl. Instrum. Methods Phys. Res. A* **2007**, *580*, 451.

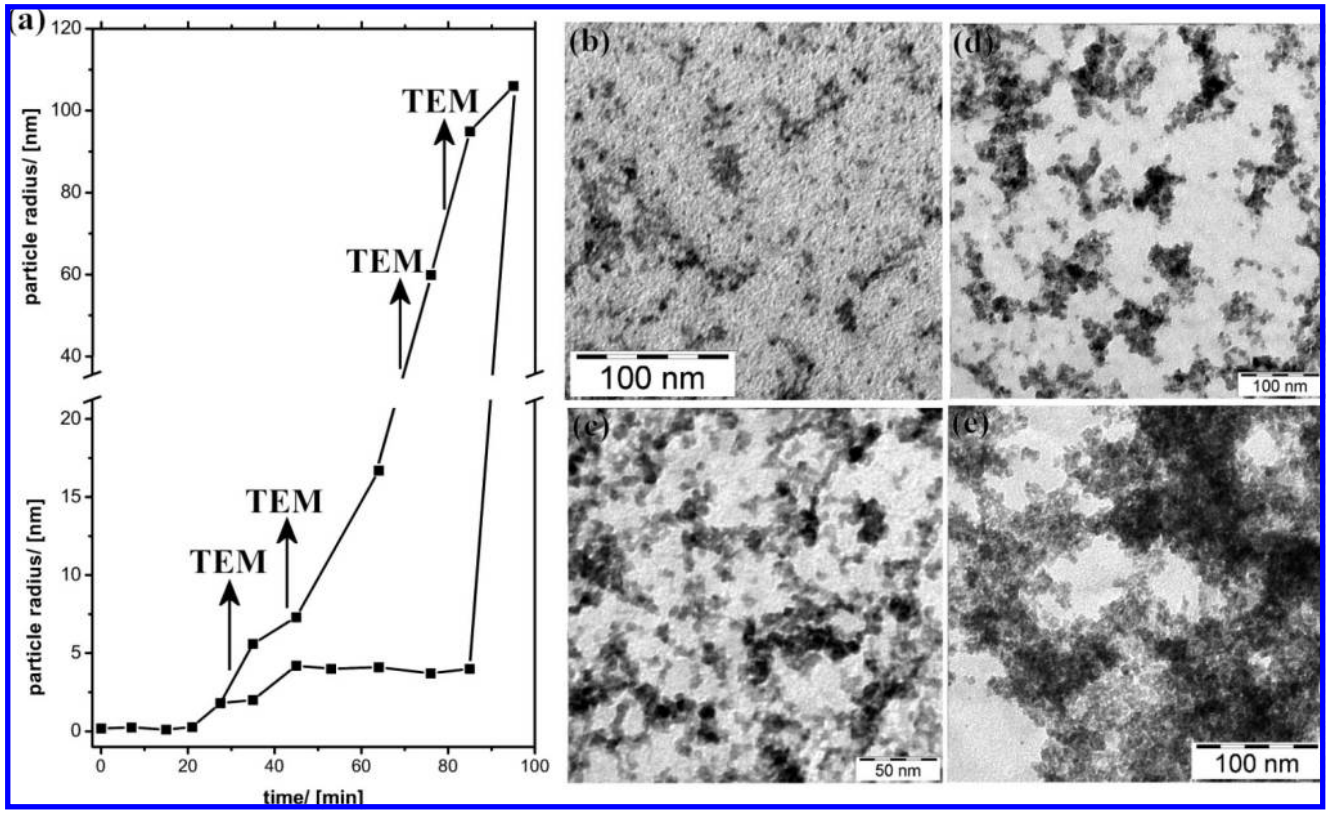


***Figure 7.*** (a) Particle sizes determined from DLS measurements as a function of time for the reaction of $[MeZnO^{tert}Bu]_4$ ($c = 3 \cdot 10^{-3}$ mol/L; $T = 10$ °C) with water. (b) TEM micrographs of samples taken at different stages in the growth process. $t = 30$ min (b), $t = 43$ min (c), $t = 66$ min (d), $t = 78$ min (e).

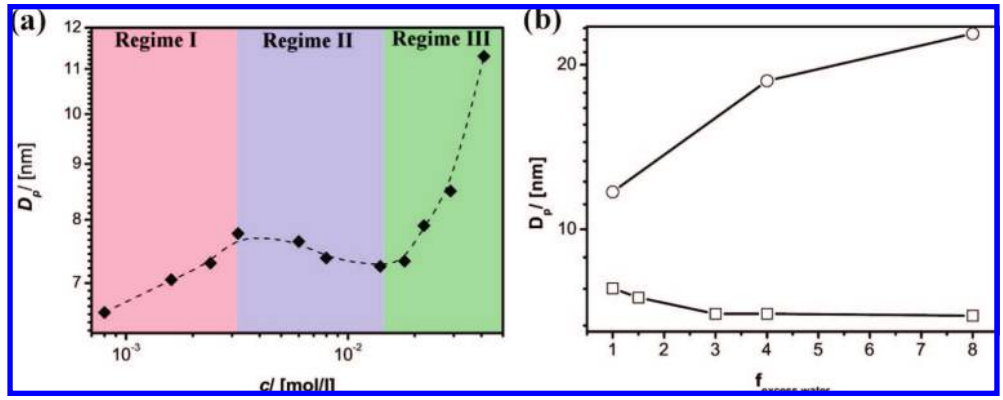


***Figure 8.*** (a) Particle size determined from PXRD measurements depending on the concentration of $[MeZnO^{tert}Bu]_4$. (b) Effect of an excess of water on ZnO growth for the two regimes; regime II (□), regime III (○).

a high number of very small particles in the size-range $D_p \approx 4$ nm are present.

At $t = 43$ min growth has occurred and only particles with $D_p = 7-8$ nm can be seen. The aggregation degree is still relatively low. In the following the size of the primary particles changes not significantly but the agglomeration is strongly enhanced, until at $t = 78$ min only large agglomerates and no free particles can be seen.

**Dependence of ZnO Formation on External Parameters.** It was shown in the previous section that flocculation effectively interrupts the growth process of the single ZnO particles. The investigation of the primary particles size in the precipitated ZnO materials by PXRD allows the investigation of the effects of different parameters (concentration of reactands, temperature and solvent) on growth processes. In order to obtain reliable information about the particle size after growth PXRD data were collected and the diffractograms were evaluated using a refined Warren-Averbach examination (see Supporting Information S-6) which is much more precise than the analysis of the width of singe reflexes using the Scherrer method.

First experiments were performed at different concentrations of $[MeZnO^{tert}Bu]_4$ and corresponding amounts of $H_2O$. The size of the primary particles was determined from PXRD analysis of the precipitates formed during phase IV (compare to Figure 2c). It is seen that there is no simple relation between the concentration of the reactands and the ZnO particle size (Figure 8). Three regimes can be identified. At very low reactant concentration the particle size increases slightly when the concentration is elevated. After nucleation there is not enough heterocubane left to lead to significant growth. Surprisingly, the ZnO particle size decreases again although the precursor concentration is now higher in regime II. This unusual behavior

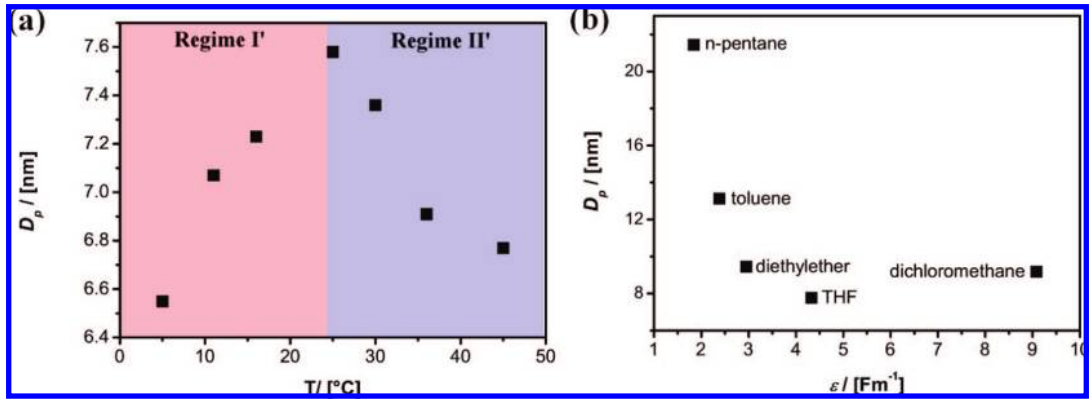


***Figure 9.*** (a) Dependence of the ZnO particle size from the temperature applied for the reaction of $[MeZnO^{tert}Bu]_4$ with water, and the effect of different solvents.

can be explained if one considers the number of critical nuclei $N(r^*)$ and its dependence on concentration (eq 7):

$$N(r^*) = C \cdot \exp\left(-\frac{G(r^*)}{RT}\right) = C \cdot \exp\left(-\frac{\frac{16\pi\gamma^3_{\mathrm{ZnO-solv}}V^2_{\mathrm{m}}}{3(RT\ ln\ S)^2}}{kT}\right) \quad (7)$$

with $G(r^*)$ being the free enthalpy of the critical nuclei, $\gamma_{\mathrm{ZnO\text{-}Solv}}$ being the interfacial tension between ZnO and the solvent, $V_m$ being the molar volume, and $S$ being the supersaturation. A higher concentration of reactands leads to a faster reaction (compare to eq 3). This in turn means that a higher supersaturation is reached in less time (see Figure 3b), respectively the supersaturation will become high. At higher values for $S$ a larger number of critical nuclei are formed and among those the remaining amount of ZnO "hidden in the remaining precursor" is shared during growth. Regime II can therefore be characterized as the nucleation dominated regime. As a result, because more and more particles are formed the particle size decreases in regime II until sufficient precursor is present to feed the growth process. Then, in regime III which might be called the growth-dominated regime, the number of critical nuclei formed is less important. Significant growth takes place and the particle size increases again. The two regimes II and III react very different to the presence of an excess of water (Figure 8b). An excess of water will also lead to an enhancement of the reaction rate (see eq 3). In regime II the latter leads to more critical nuclei formed and according to the same arguments mentioned above to a slight decrease in ZnO particle size. On the other hand, if there is plenty of ZnO precursor present (regime III) the increase in reaction speed also by water induces a significant growth of the particles.

A complex behavior is also seen when the reaction is conducted at different temperatures (Figure 9a). Similarly to the concentration dependence there are two regimes seen. In regime II′ the particle size drops with increasing temperature due to comparable arguments mentioned above: With increasing temperature, the reaction speeds up (see Figure 3a), and as a result the same amount of ZnO becomes distributed among a larger number of particles. The decrease of particle sizes with decreasing temperature however must be connected to a different effect (regime I′). At the current point we are not absolutely sure about the factors playing a role here. However, we suppose that the situation is similar to regime I (Figure 8a). The reaction is so slow at low temperatures that although less critical nuclei are formed they are not sufficiently fed to ensure significant growth.

Finally, the effect of different solvents on the ZnO particle size was investigated. The result (see Figure 9b) is rather surprising. The ZnO particle size seems to depend on the polarity of the solvent expressed as the dielectric constant $\varepsilon$. It seems that the ZnO grows more in an apolar solvent like in *n*-pentane ($D_p = 21.5$ nm) in comparison to a more polar solvent like THF ($D_p = 7.7$ nm). The explanation for this unusual behavior is probably again the number of critical nuclei formed. $N(r^*)$ depends strongly on $\gamma_{\mathrm{ZnO\text{-}Solv}}$ (see eq 7). A solvent of low polarity cannot interact so well with the forming, highly polar ZnO crystal. $\gamma_{\mathrm{ZnO\text{-}Solv}}$ will be high for nonpolar solvents, and according to eq 8 $N(r^*)$ will also be small. Then, the increase of particle size in nonpolar solvents can be explained by the nucleation-dominated regime situation (see above). Although dichloromethane possesses a very high polarity, the resulting particle size is slightly higher compared to THF as a solvent. This indicates that more factors than only polarity are important, for instance the ability of a solvent to interact with the growing ZnO nuclei by coordinative bonds. $CH_2Cl_2$ is in contrast to THF a noncoordinating solvent. It cannot stabilize the ZnO surfaces by a specific Lewis-base-acid interaction with low coordinated $Zn^{2+}$ centers. Therefore, $\gamma_{\mathrm{ZnO\text{-}CH_2Cl_2}}$ will be larger than $\gamma_{\mathrm{ZnO\text{-}THF}}$, the number of critical nuclei will be smaller, and the particles will grow larger.

## Conclusion

Organometallic methylzinc alkoxide heterocubanes were investigated as versatile precursors for the synthesis of ZnO in organic solvents. It could be shown that nanocrystalline ZnO particles could be formed even at temperatures below room temperature with water as a reactant. Furthermore, it was demonstrated that the reactivity of the precursors can be tuned in such a way that the entire process becomes slow enough to use standard analytical tools for the in situ investigation of ZnO nucleation and growth. Several interesting findings are reported. The strong impact of the alkoxide group was clarified by the mechanism of the reaction of $H_2O$ with $[MeZnOR]_4$. Unexpectedly, the alkoxide group becomes cleaved prior to the $Zn-CH_3$ group. The occurrence of a relatively stable intermediate in which OH represents one edge of the "$Zn_4O_4$" core was postulated. The consumption of the intermediate leads to the formation of new Zn−O−Zn bonds, resulting in a raise of supersaturation. Critical nuclei are formed which are of the order of ∼1.5nm in size and have Wurtzite structure. The conditions under which the following growth of ZnO occurs are dictated mainly by the precursor concentration. At "medium" concentra-

tions the growth is influenced mainly by the number of critical nuclei which emerge during the initial period. Interestingly, in this nucleation dominated regime the choice of solvent is most important. At otherwise constant conditions the largest particle were found in solvents least compatible with ZnO and its surfaces. The situation changes when the concentration is either lowered or increased significantly. For very high concentration of heterocubanes, although due to the rapid reaction a high number of critical nuclei are present large particles form. In this growth dominated regime the particles grow proportional to heterocubane concentration. At very low precursor concentrations, despite the limited number of critical nuclei, there are not enough ZnO embryos left for further growth. Therefore, in this third regime particle size increases as well with increasing concentration.

## Experimental Section

All starting compounds were received from Aldrich, were purified and carefully dried prior to use. All reactions were performed under strict exclusion of air and humidity using Schlenck technique.

**Preparation of $ZnMe_2$.** $ZnCl_2$ is dried via the treatment with $SOCl_2$ under reflux. Remaining $SOCl_2$ is removed in vacuum. A solution of $CH_3MgI$ (1.25 mol) in *n*-$Bu_2O$ is slowly added to the $ZnCl_2$ (0.57 mol) under vigorous stirring. The suspension is heated for 60 h at 60 °C under reflux. The $ZnMe_2$ (bp = 43 °C) is collected by distillation in the temperature range 130−160 °C; 40.8 g $ZnMe_2$ is obtained in 75% yield.

**Preparation of the Precursors $[MeZnOR]_4$.** $ZnMe_2$ is diluted with freshly dried and distilled toluene. The solution is cooled to −78 °C. An equimolar amount of alcohol in toluene is added dropwise. The solution is warmed to RT and stirred for 12 h. The toluene is removed in vacuum. The resulting white solid is taken up in dry hexane. Residual solid products are separated by Schlenck centrifugation. The pentane is removed from the solution by vacuum drying.

**Analytic Techniques.** NMR-spectra were acquired on a Varian Unity INOVA 400 spectrometer. Raman spectra were performed on a Perkin-Elmer Raman station 400 Raman Spectrometer. IR spectra were performed on a Perkin-Elmer Spectrum 100 FT-IR spectrometer using a Perking Elmer Universal ATR sampling accessory. X-Ray diffraction was performed on a Bruker AXS D8 Advance diffractometer using $Cu_{k\alpha 1}$ radiation and a Bruker AXS Sol-X solid state energy dispersive detector position. The UV/vis measurements were done on a Varian Cary 100 scan UV/vis spectrophotometer. The DLS experiment was performed on a Viscotek 802DLS. TEM images were acquired on a Zeiss Libra 120 at 120kv acceleration voltage. The TEM-samples were prepared by dropping a drop of the reaction solution on a a carrier covered with a holy carbon foil (Plano company, S160A3). Fluorescence spectra were measured on a Varian Carey Eclipse instrument. The absorption edges of Zn at 9659.0 eV was measured at beamline ID26 (ESRF, Grenoble (F)). The spectra $\mu(k)$ were measured in transmission mode using photodiodes. The energy was calibrated immediately prior to the measurement using a zinc metal foil. Prior to measurement, the reaction was initiated by adding solutions of Zn-cubane in dry THF and $H_2O$ in THF under vigorous stirring. An aliquot of the reaction mixture was transferred after a few seconds to the measurement cell (see Supporting Information S-9), which was then placed in the beam. In order to slow the reaction sufficiently for its progress to be monitored by XAS-measurement, the cell was actively cooled to a constant temperature of 5 °C. XANES data were taken continuously during the ongoing reaction, whereas the full EXAFS were only measured at the initial, intermediate and final stage of the reaction (denoted $t_1$, $t_2$ and $t_3$, respectively). Data treatment was carried out using the software package VIPER.[35] For background subtraction a Victoreen polynomial was fitted to the pre-edge region. A smooth atomic background $\mu_0(k)$, was evaluated using smoothed cubic splines. The radial distribution function $FT[k^2\chi(k)]$ was obtained by Fourier transformation of the $k^2$-weighted experimental function $\chi(k) = (\mu(k) - \mu_0(k))/\mu_0(k)$ multiplied by a Bessel window.

**Acknowledgment.** In memory of Dr. B. Jahn. Grillo-Werke AG/Grillo Zinkoxid GmbH is most gratefully acknowledged for financial support. The Deutsche Forschungsmeinschaft (DFG) is acknowledged for funding (Project SP780/4-1: Collaborative research center SFB558). We acknowledge the European Synchrotron Radiation Facility for provision of synchrotron radiation facilities, and we thank Dr. Marcin Sikora and Dr. Pieter Glatzel and for assistance in using beamline ID26. We also gratefully thank Dr. O. Tkachenko for her relentless support of our work. We thank A. Kuschel for helping us with TEM measurements and U. Haunz for help with the in situ NMR measurements. Prof. Dr. H. Brintzinger is acknowledged for valuable discussions.

**Supporting Information Available:** S-1: $^1$H NMR data for the prepared heterocubanes; S-2: Scheme of the excluded, molecular mechanism; S-3: Time-dependent FT-Raman spectra; S-4: Raman spectra of the used heterocubanes; S-5: Determination of the extinction coefficient for ZnO in homogeneous solution; S-6: Band-gap versus particle size; S-7: Time dependent fluorescence spectra; S-8: TEM images recorded during nucleation and growth; S-9: XAS sample cell. This information is available free of charge via the Internet at http://pubs.acs.org.

JA804071H

(35) Klementiev, K. V. *VIPER for Windows*; 2005.